Check for updates

Implications of groundwater development and seawater intrusion for sustainability of a Mediterranean coastal aquifer in Tunisia

Adel Zghibi ● · Ali Mirchi · Lahcen Zouhri ·
Jean-Denis Taupin · Anis Chekirbane ·
Jamila Tarhouni

Abstract Tunisia relies extensively on coastal groundwater resources that are pumped at unsustainable rates to support irrigated agriculture, causing groundwater drawdown and water quality problems due to seawater intrusion. It is imperative for the country to regulate future groundwater allocations and implement conservation strategies based on robust hydrogeological assessments to alleviate the adverse impacts of groundwater depletion. We developed a 3D transient density-dependent groundwater model by coupling MODFLOW-2000 and MT3DMS to improve understanding of seawater intrusion into the Korba aquifer in Tunisia. Results indicate that groundwater overexploitation since 1965 induced 5.15 Mm^3/year of seawater inflow while reducing submarine discharge into the sea by about 9.74 Mm^3/year as compared to the steady state water budget in 1965. Projecting withdrawals from 2014 up to 2050 results in a slow but extensive groundwater table decline forming a cone of depression 15 m below sea level. The seawater wedge under this business-as-usual scenario is expected to reach 1.8 km from the shoreline, causing significant mixing of the TDS-rich seawater in the aquifer system. The cone of depression under a 25% increase in groundwater withdrawal drops to about 20 m below sea level while the saltwater front reaches 2.5 km inland. Countering the seawater intrusion problem requires reducing groundwater pumping by 17 Mm^3/year to push back the saltwater front along the coastline by about 25% over a 43-year period. Application of the presented generic groundwater simulation framework guides developing management strategies to mitigate seawater intrusion in the Korba coastal aquifer and similar areas.

A. Zghibi (✉)
Faculty of Sciences of Tunis, UR13ES26, University of Tunis El
Manar, 2092 Tunis, Tunisia
e-mail: adelzguibi@yahoo.fr

e-mail: adel.zghibi@fst.utm.tn

A. Mirchi
Department of Biosystems and Agricultural Engineering,
Oklahoma State University, 111 Agricultural Hall, Stillwater, OK
74078, USA

L. Zouhri
AGYLE, SFR Condorcet FR CNRS 3417, Polytechnic Institute
UniLaSalle Beauvais, 19 Pierre Waguet Street, 60026 Beauvais,
France

J.-D. Taupin
Hydrosciences, UMR 5569 (IRD, CNRS, UM1, UM2),
Montpellier, France

A. Chekirbane
Georesources Laboratory, Water Research and Technology Centre,
Borj Cedria Ecopark 8, PO Box 273, 8020 Soliman, Tunisia

J. Tarhouni
National Institute of Agronomy, University of Carthage,
1082 Tunis, Tunisia

Introduction

Tunisia is facing fundamental water management challenges like many other countries in the Middle East and North Africa (MENA) region and around the globe where irrigated agriculture is practiced in arid/semi-arid coastal areas (Rahman et al. 2013; Droogers et al. 2012; Yazdanpanah et al. 2014). Climate change is projected to adversely affect Tunisia's water resources, a problem that is expected to occur in the Western Mediterranean region in general (Kerrou et al. 2010; Verdier 2011; Kajenthira et al. 2012; UN-Water 2014; Tsujimura et al. 2014; Lachaal et al. 2016). This challenge is compounded with increased urban water demand associated with population growth, as well as greater agricultural water demand due to prolonged growing seasons (Paniconi et al. 2001; Don et al. 2006; Kerrou et al. 2010; Rahman et al. 2013; Chekirbane et al. 2016; Zghibi et al. 2016). To cope with the growing mismatch between natural surface water supply and water demand, the country has relied extensively on groundwater resources that are pumped at unsustainable rates.

Tunisia's coastal aquifers at the Mediterranean Sea are in great need of appropriate regulatory and socioeconomic instruments to support sustainable agriculture (El Ayni et al. 2013). Many coastal zones, including the Cap-Bon Peninsula in northeastern Tunisia, have fragile environmental systems that are susceptible to anthropogenic impacts such as aquifer overexploitation, causing groundwater table decline and groundwater quality issues (i.e., salinization) due to seawater intrusion (e.g., Werner and Gallagher 2006; Kerrou et al. 2010; Zghibi et al. 2014a; Chekirbane et al. 2016; Liang et al. 2019). Groundwater plays a critical role in sustaining irrigated agriculture in the Cap-Bon region by buffering surface water variability and shortages during droughts. The region is one of the most productive agricultural areas in Tunisia, contributing about 15% of Tunisia's total agricultural production (CCI Cap-Bon 2018).

Quantitative understanding of the various factors affecting groundwater flow and solute transport processes are essential for sustainable groundwater resource development and operation of coastal well fields. Numerical simulations have become a practical tool for informed coastal groundwater management (Bear et al. 1999; Chandio and Lee 2012; Doulgeris and Zissis 2014; Xu et al. 2015; Liang et al. 2019) by improving understanding of the spatial extent and rate of seawater intrusion (e.g., Kerrou et al. 2010; Salcedo-Sànchez et al. 2013; Chekirbane et al. 2015). The primary benefit of numerical modeling is providing a means to analyze spatial and temporal dynamics of groundwater flow and saltwater movement in coastal aquifers using simplified conceptual representations of key features of complex aquifer systems (Hill and Tiedeman 2006; Chen et al. 2017; Xu et al. 2018). Thus, they facilitate diagnosis of the main drivers of groundwater table decline (e.g., regional water management, agricultural water use, and/or climate change) and salinization due to changes in groundwater pumping and recharge conditions. Coupled groundwater models (e.g., coupled MODFLOW - MT3DMS) allow simultaneous simulation of dynamic flow and solute transport processes. However, coupled modeling frameworks are typically complex and computationally intensive (Post 2005; Werner et al. 2013; Liang et al. 2019). Different analysis methods have been developed to address this weakness, including scenario-based simulation of the hydrodynamic equilibrium between freshwater/seawater interface (Langevin and Guo 2006; Mao et al. 2006; Kamali and Niksokhan 2017; Don et al. 2006).

This paper presents a coupled numerical groundwater modeling framework to quantify groundwater drawdown and seawater intrusion into coastal aquifers based on robust hydrogeological assessments. We used field surveys and monitoring data, mathematical modeling, and simulating groundwater management scenarios to characterize long-term vulnerability to seawater intrusion and the required effort to mitigate the problem in the Korba unconfined aquifer system in Tunisia's Cap-Bon Peninsula. We linked MODFLOW-2000 (Anderson and Hill 2000) and MT3DMS (Qahman and Larabi 2006; Langevin and Guo 2006) models within the Groundwater Modeling System (Xiaobin 2003) to examine necessary measures to restore groundwater quantity and quality through a series of pumping simulations. Numerical models of groundwater flow and solute transport (i.e., the propagation of total dissolved solids (TDS) in the aquifer) help evaluate the effectiveness of different groundwater management scenarios. The linkage of the three-dimensional (3D) variable density simulation of seawater intrusion with transport techniques provides a powerful method for simulating the aquifer under various types of boundary and initial conditions, objective functions, and operational constraints.

Materials and methods

Study area and problem setting

The Korba aquifer (440 km^2) is located between Nabeul and Kélibia cities in northeastern Tunisia. It is bounded in the east by the Mediterranean Sea and in the west by the Sidi Abderrahmen anticline (Fig. 1). The aquifer is comprised of two distinct formations: a Pliocene sandstone spanning the entire aquifer and a Quaternary alluvium containing sand, gravel, silt, and thin clay lenses in the southwest (Ennabli 1980). An important geomorphologic feature in the area is the presence of a dune formation of high-transmissivity Quaternary sediments running parallel to the coastline, separating the Korba plain from the sea (Ennabli 1980; Kerrou et al. 2010; Chekirbane et al. 2015). The region's main coastal salt flats, known as sabkhas, are the natural outlets of the Tyrrhenian which receive permanent discharges of treated wastewater and occasional exchanges with the sea (El Ayni et al. 2013). The clay bottom of sabkhas limits their interaction with groundwater.

The aquifer is naturally recharged by rainfall infiltration, which is larger in the river beds and in the dune and smaller in the Quaternary areas (Kerrou et al. 2010; Zghibi et al. 2014b). The topography is characterized by a gentle slope (0–15%) over most of the study area but, locally, slopes steeper than 15% are observed. The climate is semi-arid with Mediterranean influence characterized by moderate winter precipitation. Mean annual temperature is 17 °C with a minimum of 6.1 °C in January and a maximum of 37 °C in July. Mean annual rainfall during the last decade was 420 mm. The dry period (average rainfall, 150 mm) spans nine months, peaking in June/July.

The region is home to about 145,000 inhabitants. The main economic activities are tourism and irrigated agriculture (CCI Cap-Bon 2018). The principal crops are strawberries (300 ha), potatoes (1200 ha), tomatoes (3500 ha), peppers (3500 ha), and other vegetables (1500 ha). Although agricultural activities and agro-industries dominate, host food industries, textile, dairy, and paper industries are also present. Water demand for irrigation is met mainly from the shallow aquifer exploitation and by surface water from the water supply canal between the Medjerda River and Cap-Bon Peninsula.

In the last decade, hydrogeological studies have indicated three main problems linked to the extensive agricultural activities in the study area: (1) rapid growth of agricultural lands despite limited water resources and deteriorating groundwater quality (Kerrou et al. 2010; Zghibi et al. 2014a; Chekirbane et al. 2015); (2) intensive well pumping due to significant expansion of irrigated area (Zghibi et al. 2014a); and (3) soil salinization due to the effect of fertilizers (nitrogen, phosphorus, and potassium), high evaporation rate, and, especially, excessive irrigation return flow (Zghibi et al. 2014b).

The Korba aquifer exploitation has greatly increased since the 1960s (Ennabli 1980), from 400 wells pumping 2.5 Mm^3 in 1965 to more than 13000 wells pumping 68 Mm^3 in 2014 (Fig. 2). The distribution of the wells is particularly dense towards the coastal part of the agricultural plain, which tends to accentuate the inland movement of the freshwater-saltwater interface.

Figure 3a and b present piezometric level maps in 1965 and 2014, which illustrate the effect of groundwater development to support agricultural production. The region is presumed to have had a stable, smooth potentiometric surface located above sea level up to the 1960s prior to the onset of an era of economic growth and groundwater development.

By contrast, the 2014 piezometric map of the Korba area shows a cone groundwater of depression of 12 m below sea level observed at 3000 m from the Mediterranean shoreline (Fig. 3b) mainly between the villages of Tafelloun and Diarr-El-Hojjaj. Likewise, a localized piezometric depression of up to 5 m below sea level is observed in the western part. Nearer to the shoreline, the piezometric level contours become increasingly negative. The piezometric levels are highest in the left part of Lebna Dam (built in 1986) and Chiba Dam (built in 1963), as well as in the south near Somâa village. The two dams have a positive impact on the recharge of the aquifer by increasing infiltration and percolation. Figure 3b shows Diarr Hojjaj piezometric depression and the seaward orientation of groundwater flow. The reversal of groundwater flow direction due to the regional piezometric depression and saltwater up-coning chiefly in the central depression zone are two major processes controlling seawater intrusion in the study area.

Chloride (Cl$^-$) is the main chemical constituent of concern in the coastal aquifer and the most commonly used indicator of mixing brackish water derived from
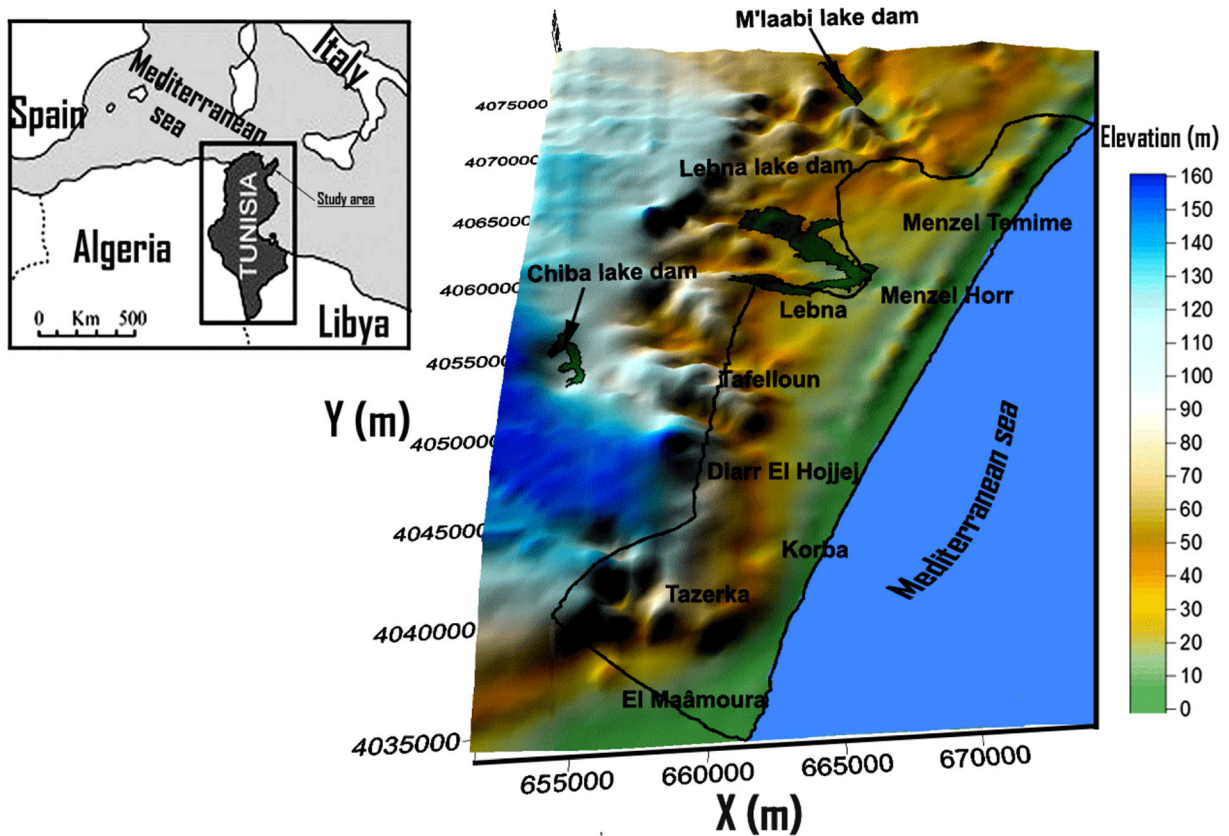
**Fig. 1** Location of Tunisia and topographic map of the Korba study area

the sea (Nettasana et al. 2012). Historical shallow groundwater chloride concentrations from Korba aquifer have been evaluated for data quality and temporal trends. The chloride concentration gradually increased between 1965 and 2014 (Fig. 4). In the 1960s, chloride concentrations were relatively low (generally < 400 mg/l) throughout the region, with a few exceptions, especially in the north of Korba (Fig. 4a). During the 2014 monitoring period, almost all the samples had elevated Cl⁻ concentrations (Fig. 4b) ranging between 300 and 6000 mg/L. Most of the areas with elevated Cl⁻ concentrations are near the Mediterranean Sea and in the central part of the aquifer at 1.55 km inland had Cl⁻ values

between 6000 and 15000 mg/L. The spatial distribution of chloride contamination is clearly correlated with the lowering of piezometric levels, which can be ascribed to groundwater overdraft and/or a natural decrease in groundwater recharge (Zghibi et al. 2011). The salinization of groundwater is linked to geochemical processes such as the presence of direct cation exchange and dissolution processes (halite, dolomite, and gypsum) associated with cations exchange (e.g., Paniconi et al. 2001; Kerrou et al. 2010; Zghibi et al. 2014a, b; Chekirbane et al. 2015). Nevertheless, seawater intrusion is the major source of groundwater contamination in the Korba coastal plain.

Fig. 2 Time Evolution (1965–2014) of number of wells, groundwater exploitation and recharge
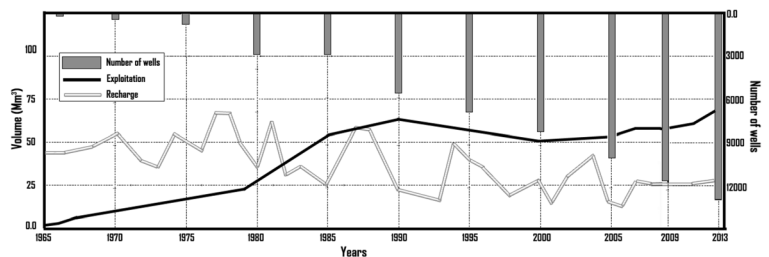
Fig. 3 Potentiometric map evolution of the Korba aquifer and flow direction: **a** 1965 (Ennabli 1980) and **b** 2014 (Chiba built in 1963; M'Laabi built in 1964 and Lebna built in 1986)
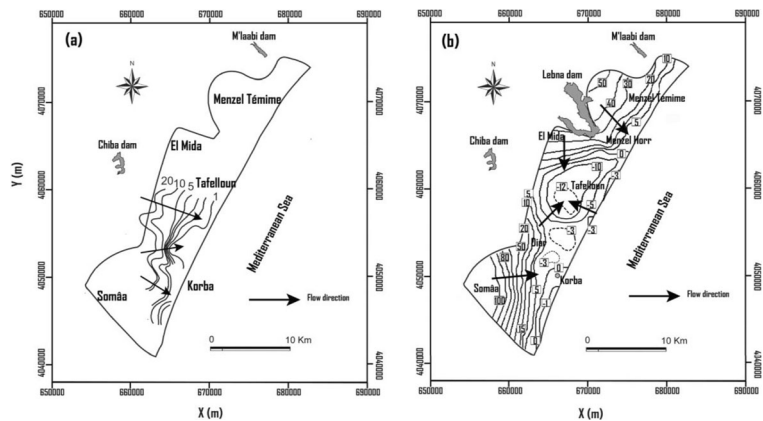
Modeling approach

Numerical model

We applied Groundwater Modeling System (GMS 6.5) (AQUAVEO 2018) to simulate flow and transport in the coastal environments of the Korba plain. GMS 6.5 package uses a modified version of MODFLOW-2000 to solve the differential equation that governs the flow in a porous medium and three-dimensional multi-species transport model MT3DMS to solve the solute transport equation.

The partial differential equation of groundwater flow used in MODFLOW is as follows (McDonald and Harbaugh 1988):

$$\frac{\partial}{\partial x}\left(K_{xx}\frac{\partial h}{\partial x}\right)+\frac{\partial}{\partial y}\left(K_{yy}\frac{\partial h}{\partial y}\right)+\frac{\partial}{\partial z}\left(K_{zz}\frac{\partial h}{\partial z}\right)-W$$
$$=S_S\frac{\partial h}{\partial t} \tag{1}$$

where h = the piezometric head (L); K_{xx}, K_{yy}, and K_{zz} = the hydraulic conductivity along various axes (x, y, z) (LT^{-1}); W = sources and/or sinks of water represented by volumetric flux per unit value; S_S = specific storage (L^{-1}); and t = time.

The equation for solute transport in hydrodispersive modeling (e.g., Anderson and Woessner 1992; Bear and Cheng 2010) is described below:

$$\frac{\partial C}{\partial t}=\frac{\partial}{\partial x_i}\left(D_{ij}\frac{\partial C}{\partial x_j}\right)-\frac{\partial}{\partial x_i}(Cv_i)-\frac{C'q}{\omega_e} \tag{2}$$

where C = the solute concentration in water (ML^{-3}), v_i = the components of the velocity vector (LT^{-1}), ω_e = the effective porosity, D_{ij} = the dispersion coefficients ($L^2 T^{-1}$), C' = a known source concentration (ML^{-3}), q = a source/sink term (T^{-1}), and t = time.

The transport module in porous medium is mainly governed by the processes of advection and dispersion of conservative and dissolved substances. The GMS package uses a one-step lag between numerical model of flow and transport, minimizing model complexity

Fig. 4 Chloride concentration (mg/l) evolution of the Korba aquifer: **a** 1965 (Ennabli 1980) and **b** 2014 (Chiba built in 1963; M'Laabi built in 1964 and Lebna built in 1986). Increasing circle size represents increasing concentration
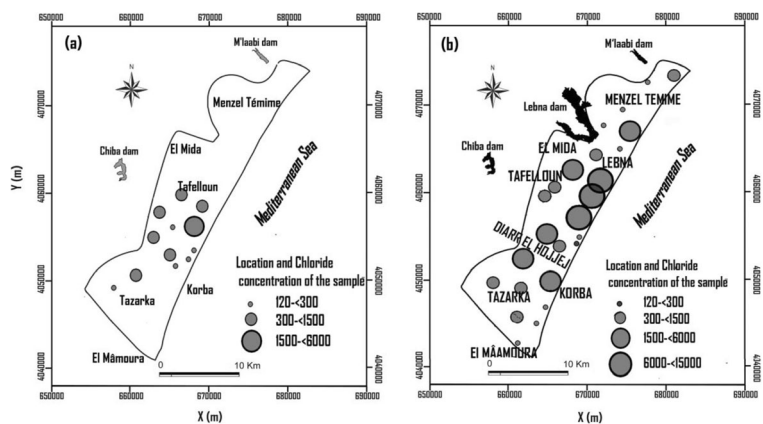
and runtime. This means that MODFLOW runs for the same time step of MT3DMS using the last simulated salt concentration from the transport model to calculate the density terms in the flow equation described by McDonald and Harbaugh (1988) and flow velocities. In the next time step, the velocities are used by MT3DMS to solve the transport equation reducing the model run time.

Aquifer geometry and boundary conditions

As described by Ahmad et al. (2010), model development in relation to a finite difference grid refers to the process in which all available data describing the field conditions are processed and interpreted in a systematic way. In this study, the aquifer geometry was determined by association of both the bedrock based on available lithological logs, geological cross sections, and the digital elevation model (DEM). The modeling process was applied to the plio-quaternary aquifer representing an alluvial and phreatic structure, covering an area of approximately 440 km^2. The plio-quaternary unit is very productive and corresponds to an alteration of marine sand with shells and sandstone with thin clay lenses. The Pliocene formation has a mean thickness of 85 m comprised of sandstone with alternating marl units. The Quaternary alluvium is composed of detrital sediments (sand, gravel, and silt) with thin clay lenses and has a thickness that varies between 20 and 25 m. Laterally, the facies changes southward to more differentiated clay, sand, and sandstone layers. The thickness of the plio-quaternary formation is about 80 m in the central part of the area, reaching 250 m offshore, and decreasing towards the west. The marls of the middle Miocene form an impermeable basement to this aquifer which acts as an aquitard (Ennabli 1980) (Fig. 5).

The piezometric map of 1965 (Fig. 1), obtained through kriging interpolation method, was used to represent the hydraulic head distribution, which is effectively the upper limit of the groundwater model. The saturated aquifer thickness was computed by subtracting the steady sate 1965 head level from the bedrock elevation.

Model boundaries were assigned based on topographic maps and hydrological field investigations. The Mediterranean Sea forms the eastern physical boundary of the model defined as a specified head boundary with a zero-assigned value. The north and south boundary conditions coincide with H'jarr and Kébir rivers (Fig. 6), respectively (Zghibi et al. 2011). These boundaries were modeled as a fixed-head condition. Furthermore, a general head condition was applied at the western end separating the Korba aquifer from the adjacent Grombalia aquifer as indicated by groundwater flow directions. The hydro-climatic processes including evaporation from the water table and recharge from mainly rivers (Lebna, Chiba, and Korba rivers) were applied to a specified head. Pumping wells were incorporated into MODFLOW Well package (Fig. 6). Finally, the Miocene bedrock corresponding to the aquifer's bottom level was defined as a no-flow boundary.

With regard to the transport problem linked to flow dynamics, the eastern boundary is considered highly important since it is in direct hydraulic interconnection with the Mediterranean Sea (Siarkos and Latinopoulos 2016). The sea boundary where concentration was set equal to 38 ± 0.03 kg/m^3 (Kotnik et al. 2017; Coro et al. 2018) was specified as a constant concentration boundary. In transport calibration, the total dissolved salts concentrations are used as a tracer for the characterization of groundwater contamination from seawater intrusion (Qahman and Larabi 2006). In addition, we used a reference water density value of 1025 kg/m^3 for seawater and 0.5 kg/m^3 for the initial concentration of freshwater. The simulation of freshwater/saltwater flow transition interface is very complex and requires an initial estimate of the interface altitude level (Pham and Lee 2015). We assumed that the initial depth location of freshwater/saltwater transition zone was at the Mediterranean seaside boundary from layer 1 to 5.

Hydrodynamic parameters

The hydrodynamic parameters were obtained from several pumping tests combined with literature values available from previous studies (e.g., Ennabli 1980; Paniconi et al. 2001; Kerrou et al. 2010; Zghibi et al. 2011). The hydraulic conductivity varies greatly ranging on average between 10^{-4} and 10^{-6} m/s, which is a common characteristic of alluvial aquifers. The largest values of hydraulic conductivity (sometimes exceeding 10^{-3} m/s) occur in the south near Somâa City whereas the areas surrounding Menzel-Témime city are characterized by moderate hydraulic conductivity (less than 10^{-4} m/s) found across about 20% of the study area. After averaging the hydraulic conductivity values for each zone, the horizontal spatial distribution of conductivity
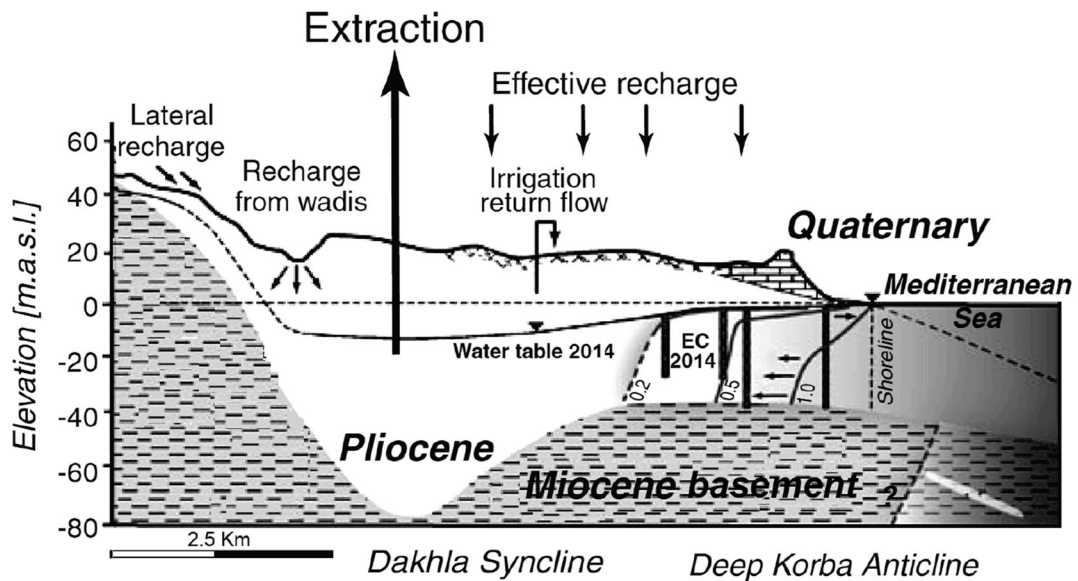
Fig. 5 Simplified hydrogeological cross section of Korba aquifer sketching the conceptual model based on up-to-date geological and hydrodynamic data (Modified from Kerrou et al. 2010)

parameter was homogenized ($K_x = K_y$) and assigned to every zone. The vertical hydraulic conductivity (K_z) was assumed to be one-tenth of the horizontal hydraulic conductivity (Table 1) (Chekirbane et al. 2015).

For the transport parameters, the effective porosity ranged between 0.2 and 0.24 based on measurements of distribution of subsurface resistivity (Zghibi et al. 2014b). Vertical hydraulic conductivity anisotropy and

Fig. 6 Distribution of wells with pumping rates and drainage network in the Korba area (Modified from Kerrou et al. 2010)
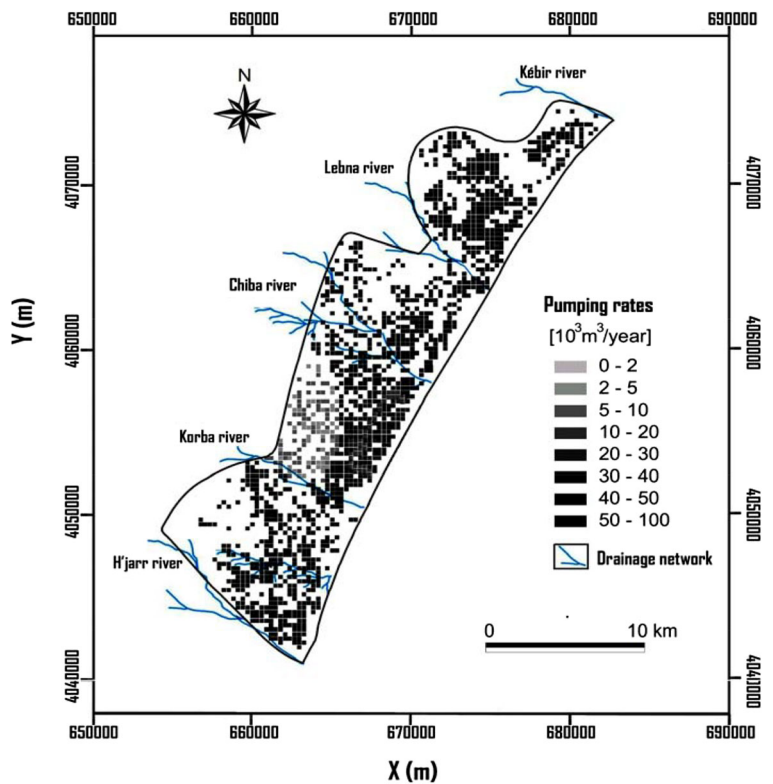
Table 1 Model input parameter values

Characteristics of the Korba aquifer flow model

Simulated surface area	440 km^2 (length: 40 km; width: 11 km)
Spatial discretization	Finite differences grid (rows: 110; columns: 100) on a geological map (scale 1/25000)
Vertical discretization	5 units (variable thickness)
Boundary conditions	Assigned to the model based on topographic maps and field investigations
Initial conditions	Hydraulic head configuration of the year 1965 (for the steady state) and hydraulic head configuration for the year 2014 (for the transit sate) state)

Hydraulic parameters

Zone	K_x(m/s)	K_y(m/s)	K_z(m/s)	D_L(m)	D_T(m)	Porosity	S_s (m^{-1})
1	0.5×10^{-4}	0.5×10^{-4}	0.5×10^{-5}	15	1.5	0.2	10^{-5}
2	6×10^{-4}	6×10^{-4}	6×10^{-5}	10	1.0	0.24	10^{-5}
3	3×10^{-4}	3×10^{-4}	3×10^{-5}	4	0.4	0.23	10^{-5}
4	7×10^{-4}	7×10^{-4}	7×10^{-5}	10	1.0	0.21	10^{-5}
5	5×10^{-5}	5×10^{-5}	5×10^{-6}	15	1.5	0.2	10^{-5}
6	0.5×10^{-4}	0.5×10^{-4}	0.5×10^{-5}	7	0.7	0.2	10^{-5}
7	2.5×10^{-4}	1.5×10^{-4}	0.5×10^{-5}	6	0.9	0.2	10^{-5}

$K_x = K_y$ horizontal hydraulic conductivity, K_z vertical hydraulic conductivity, S_s specific storage, D_L longitudinal dispersivity, D_T transversal dispersivity

vertical leakance vary, respectively, from 3 to 15 and 0.02 to 0.25 (Kerrou et al. 2010). Commonly, horizontal transverse dispersivity is 20 to 10% of the longitudinal dispersivity (e.g., Giambastiani et al. 2007; Cobaner et al. 2012; Siarkos and Latinopoulos 2016). The numerical domain was divided into seven hydrodynamic zones whose parameters were calibrated separately (Fig. 7a), with the exception of specific storage (Table 1), which was assumed to be homogenous throughout the aquifer.

Recharge conditions and groundwater abstraction

The Korba plain's aquifer system is primarily recharged by precipitation (Fig. 8a). The net recharge by infiltration of rainfall was estimated to be up to 10% of the 420 mm/year mean average precipitation (e.g., Ennabli 1980; Paniconi et al. 2001). In flow/transport modeling, a specified low salt concentration of 0.085 kg/m^3 was applied for surface recharge from rainfall. Furthermore, the aquifer is recharged by infiltration from ephemeral streams (wadis) across the plain from northeast to southwest, including approximately 3.7 Mm^3/year and 1.6 Mm^3/year from Lebna and Chiba wadis, respectively. Three wadis of Chiba, M'laabi, and Lebna were dammed in 1963, 1964, and 1984, respectively, for artificial recharge of the aquifer (approximately 1 Mm^3/year) by capturing floods.

Additional sources increase total aquifer recharge in the Korba plain. Recharge from the irrigation return flow is significant, especially for the shallow groundwater with a low initial water table. Kerrou et al. (2010) estimated the infiltration from irrigation return flow at 16% (8 Mm^3/year) of the applied irrigation water (assuming 50 Mm^3/year). Another source of recharge is the Korba-El-Mida recharge site located approximately 300 m north of Korba City wastewater treatment plant. This plant, which can treat 7500 m^3 of wastewater per day, started operating in July 2002, and it presently receives about 5000 m^3/day. The recharge site went into operation in 2008 with three infiltration ponds of $50 \times 30 \times 1.5$ m that collectively contribute about 1.7 Mm^3 of recharge per year.

The intensive groundwater abstraction represents a major water output from the aquifer system, which is about twice the amount of recharge. Groundwater withdrawal has been rising steadily (Fig. 2) despite augmenting surface water supplies by damming the wadis, encouraging farmers to adopt drip irrigation, and providing additional surface water via the Medjerda Cap-Bon Canal from the north of the country to Cap-Bon peninsula. Artificial recharge by direct infiltration of surface water from the Medjerda Cape-Bon canal and dams started in 1999 but never exceeded 1 Mm^3/year (Kerrou et al. 2010). Average annual pumping rate from
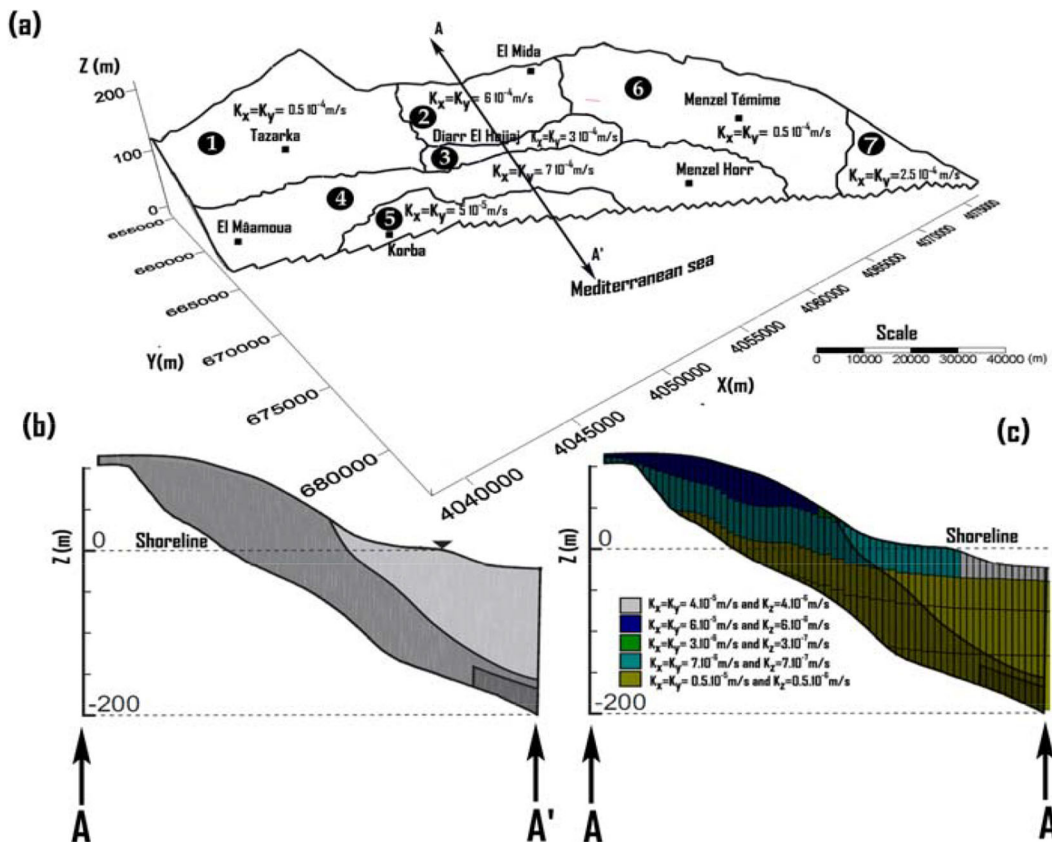
Fig. 7 **a** Hydraulic conductivity for each individual zone, **b** vertical cross section and **c** vertical hydraulic conductivity distribution cross section

a single grid cell (250 × 250 m) was estimated to vary from 1500 to 73,700 m^3/year. Groundwater pumping is assumed to start in the 1960s, increasing linearly until the 1980s. Since 2014, the total abstraction volumes are assumed to fluctuate around 68 Mm^3/year. Figure 6 illustrates the heterogonous spatial distribution of pumping rates, showing the smallest rates in the western sector potentially due to relatively lower transmissivity (Kerrou et al. 2010). Finally, clay-bottomed terrain depressions (i.e., sabkhas) in the study area form a 5-km^2 strip along the Mediterranean coastline. The sabkhas (salt flats) are suspected to be insignificant net groundwater discharge zones, although their recharge dynamics has not been thoroughly investigated.

Spatial and temporal discretization

The three-dimensional model was simulated using MODFLOW 2000 (McDonald and Harbaugh 1988; Harbaugh et al. 2000). The model domain was divided into 100 columns and 110 rows, and 5 layers. The

square-shaped Finite Difference grid was horizontally oriented from north to south while the vertical dimension was distorted (Barth et al. 2007). The model layers were also discretized vertically to avoid instantaneous vertical mixing, especially near the shoreline. The grid spacing is 250 m in both the *x* and *y* directions, and the layer thicknesses are spatially variable, reaching 80 m below the sea level according to previous geophysical surveys (e.g., Kerrou et al. 2010; Zghibi et al. 2014b; Chekirbane et al. 2015).

The temporal discretization design is based on a combination of temporal resolutions of flow model (MODFLOW) and transport model (MT3DMS). It was determined by grouping time steps into selective stress periods defined before introducing the sources/sinks (Chekirbane et al. 2015), which were further divided into transport steps. Based on changes in aquifer stresses, each stress period was divided into 10 time steps. For the flow model, the length of the time steps varies from 10 to 30 days whereas the time step length for the transport model started with 1 day and it was
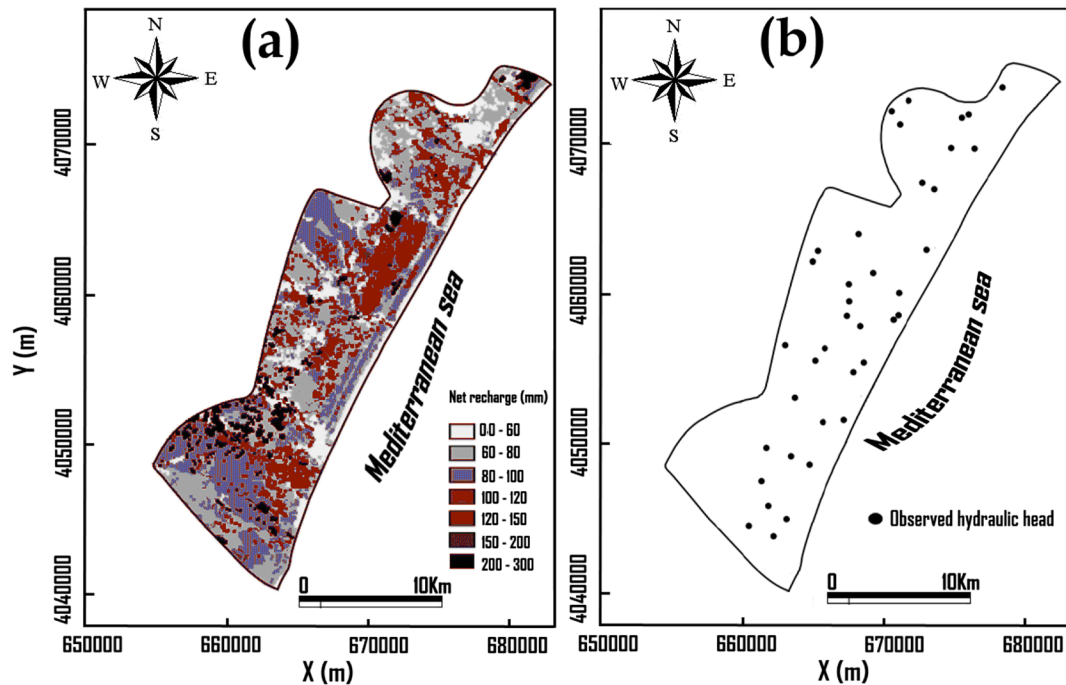
Fig. 8 **a** Spatial distribution of net recharge by infiltration of precipitation (modified from Kerrou, 2008) and **b** 38 observed hydraulic head used in the transit state calibration process

increased by applying a 1.2 multiplier factor value (Qahman and Larabi 2006).

Initial conditions

The reference piezometric level recorded in 1965 was used as an initial condition for the groundwater. This initial condition represents insignificant groundwater flow disturbance when the groundwater exploitation in the study area was negligible. The initial groundwater TDS concentration was set at 0 kg/m³, since the initial salt concentration is not known. Modeling process was performed in two steps. First, the steady state started with the above initial conditions without pumping rates in order to reproduce the initial condition for the transient state simulations by varying the hydraulic conductivities and recharge (Voss and Souza 1987). The outputs of the first simulation step were then used as initial conditions for the transient state aquifer simulation under withdrawal stress in order to characterize the storativity parameters. This was done by adding water pumping volume between 1965 and 2014 (Qahman and Larabi 2006).

Model calibration and verification

Two sequential simulation stages were carried out in the calibration phase. In the steady state calibration, the hydraulic conductivity and recharge were adjusted by trial-and-error (Doherty 2000) until the computed hydraulic heads matched the 1965 observed levels. Under transient conditions (1965–2014), the reproduction of the drawdown trend was chosen as the calibration criterion. A total of 38 calibration points were selected based on the availability of multiple time series data (Fig. 8b). For this purpose, the model parameters were checked manually by trial and error until the observed and computed heads were comparable. The hydrodynamic calibration parameters included effective porosity, specific storage, longitudinal and transverse dispersivity, and hydraulic transmissivities.

The model's performance in the calibration stage was checked using:

1. Scatterplots showing the strength of the relationship between the predicted and observed hydraulic head values defined as (Eq. 3):

$$H_s = \gamma \times H_o \Rightarrow \begin{cases} \gamma \rangle 1 \rightarrow overprediction \\ \gamma \langle 1 \rightarrow underprediction \end{cases} \qquad (3)$$

where H_s and H_o are the predicted and observed values, respectively, and γ is the slope of the regression line between the two hydraulic head datasets.

2. The mean error (ME) calculated as the average error value between the predicted and observed hydraulic head values (Eq. 4). An ME of 0 indicates a perfect fit.

$$ME = \frac{\sum_{i=1}^{N}(H_s - H_o)}{N} \qquad (4)$$

3. The mean absolute error (MAE) which measures the average magnitude of errors in a set of predictions regardless of their direction (Eq. 5):

$$MAE = \frac{\sum_{i=1}^{N}|H_s - H_o|}{N} \qquad (5)$$

4. The root mean square error (RMSE) calculated as the square root of the average of squared differences between predictions and actual observations (Eq. 6):

$$RMSE = \sqrt{\frac{\sum_{i=1}^{N}(H_s - H_o)^2}{N}} \qquad (6)$$

5. The normalized root mean square error (NRMSE) defined as the ratio of model predicted RMSE divided by the difference between H_{max} and H_{min}, respectively. NRMSE was calculated according to the following equation (Eq. 7):

$$NRMSE = \frac{RMSE}{H_{max} - H_{min}} \qquad (7)$$

After the model was successfully calibrated, it was verified by reproducing the groundwater levels in the year 2014 in the final run of the transient calibration stage. The calibrated model was then used to project the impacts of alternative groundwater management schemes up to 2050.

Groundwater management scenarios

Different groundwater withdrawal scenarios were simulated for the 2014–2050 modeling horizon in order to provide insights for mitigation and control of the seawater intrusion. The 2014 initial and boundary conditions were used for projecting the impacts of groundwater management scenarios, assuming a 2% growth in the annual groundwater withdrawal. The following scenarios were simulated:

Scenario 1: Continue the current extraction trend using average recharge conditions (1965–2014) and 2014 withdrawal rates. Scenario 1 represents business-as-usual (i.e., no mitigation policy); extraction is based only on irrigation and domestic demands.

Scenario 2: Linearly increase groundwater extraction by 25% compared to average historical pumping conditions (1965–2014). This increased pumping rate is directly proportional to the population growth and economic development. Scenario 2 is considered as a "worst-case" scenario in the current analyses.

Scenario 3: Linearly decrease groundwater extraction by 25% compared to average historical pumping conditions (1965–2014), assuming that the resulting water shortage will be compensated by developing new water resources like reuse of treated wastewater and water importation via the Medjerda Cap-Bon Canal. This scenario represents a water management scheme that prioritizes addressing the groundwater table decline and seawater intrusion by gradually reducing groundwater withdrawal.

Results and discussion

Calibration and verification

During the steady state calibration phase, the study area was divided into seven distinct zones in which hydraulic

conductivity was adjusted separately, ranging between 0.01×10^{-3} m/s and 4.2×10^{-3} m/s (Table 2 and Fig. 9). The match between the simulated and observed values indicates that the calibration criteria were met satisfactorily (Fig. 10a and Table 3). The scatter plot (Fig. 10a) illustrates a correlation coefficient (R^2) of 0.876, confirming an acceptable calibration based on the good overall fit for the hydraulic heads ($-6 < H_{obs} < 90$ m). Likewise, the MAE and RMSE values of 1.08 m and 7.658 m, respectively, are obtained after the steady state calibration, indicating an acceptable fit between the observed and calculated heads. However, the simulated heads were generally lower than the observed values based on the ME (-0.20 m) and γ (0.895). The larger values of conductivity occurred in the shoreline zones (zones 1, 3, 5 and 7) related to the highest transmissivity of about 10^{-2} m^2/s (Kerrou et al. 2010) whereas the minimum values (0.01×10^{-3} m/s and 0.07×10^{-3} m/s) were in zones 4 and 6 in the vicinity of Menzel-Témime and El-Mida villages.

For the transient state, two hydraulic parameters were included in the model inputs besides the groundwater exploitation and natural recharge: the specific storage and the artificial recharge through irrigation return flow. The correlation coefficient of 0.808, ME value of 0.43 m, γ parameter of 0.894, MAE value of 1.09 m, and RMSE value of 7.23 m indicate an acceptable transient state calibration (Table 3).

The model performance was evaluated in the verification phase by reproducing the 2014 piezometric map (Table 3 and Figs. 10b and 11a) while keeping the boundary conditions and aquifer recharge by infiltration of rainfall unchanged. With a correlation coefficient of 0.882 m and RMSE of 7.18 m, the simulated head contours illustrated the flow direction towards the concentric depression of Diarr El Hojjaj village observed at 3 km from the shoreline (Fig. 11a). This phenomenon accelerates the seawater intrusion by reversing the hydraulic gradients. Furthermore, the large head discrepancies are located in the high elevation topography in the south and the north of the Korba aquifer. These areas are characterized by steep hydraulic gradients (Nettasana et al. 2012) which was verified by the greater error factors when small changes were applied to the calibration parameters. Furthermore, reasonable agreement between the simulated and observed water tables from monitoring wells is evident from Fig. 11b.

TDS values of 17 wells, primarily located in the central part of the study area close to the piezometric depression, were considered to evaluate model performance in simulating salt transport (Fig. 12a). The R^2 and RMSE were, respectively, 0.75 and 3926 mg/L for salt concentrations ($2000 < C_{obs} < 25,000$ mg/L) indicating an acceptable liberation, although not very close (Fig. 12b). The accuracy of the salt-transport model fit could be further improved as denoted by the residual error on the plot of estimated versus measured TDS values. It is difficult to obtain a better calibration with the conceptual model used based on available data as indicated by truncation and oscillation errors in the numerical approximations of the solute transport equation.

As a preliminary check, the results of the developed 3D numerical model of density-dependent flow and miscible solute transport (Fig. 13a) were compared with perpendicular electrical resistivity tomography (ERT) carried out in the central part of the study area close to the sea (Fig. 13b). The comparison illustrates reasonable agreement between the simulated extent of the seawater wedge in 2014 and the ERT. The seawater intrusion along the Mediterranean coastline, inferred from measured resistivities (using ERT imaging), reaches 1000 m inland confirming the simulated saline transition zone (Fig. 13). Within the intruded area, most resistivity values computed by the ERT investigation are less than 2.0 ohm/m of apparent resistivity forming a transition zone between conductive seawater and resistive freshwater (Zghibi et al. 2014b). For the MT3DMS transport model, it was assumed that the extent (wedge) of seawater intrusion is widely represented by isolines of TDS equal to 2.0 kg/m^3 (Qahman and Larabi 2006).

Understanding the water budget is essential for effective water resources management in the region and also to predict future changes for a sustainable management (Dinka et al. 2014).

So, in the steady state (equilibrium condition), inflows and outflows are in balance, and the change of storage ΔS is very close to zero (i.e., 0.04). The mass balance calculated by MODFLOW 2000 showed that while 36.42 Mm^3/year of freshwater is discharged into the sea, 2.88 Mm^3/year (7.9% of the inflow) of seawater volume entered the groundwater system. The lateral recharge from the adjacent aquifer of Grombalia and from precipitation recharge in 1965 were estimated to be

Table 2 Calibrated aquifer parameter values

Zone	Steady state model		Transit state model				
	$(K_x = K_y)10^{-3}$ (m/s)	$(K_z)10^{-3}$ (m/s)	$K \times 10^{-3}$ (m/s)	n_e	$S_s \times 10^{-4}$ (m^{-1})	D_{Long} (m)	D_{Trans} (m)
1	2.4	0.32	1.1	0.28	1.1	9	0.98
2	0.3	0.05	0.15	0.03	0.4	2	0.9
3	4.2	0.39	2.2	0.27	1.9	11	1.2
4	0.01	0.0015	0.06	0.02	0.3	1	0.13
5	1.5	0.17	1.34	0.25	0.8	4	0.56
6	0.07	0.009	0.08	0.03	0.1	1	0.1
7	2.2	0.3	2.3	0.12	1.4	10	1.01

3.76 (10.3% of the inflow) and 29.82 Mm^3/year (81.8% of the inflow), respectively.
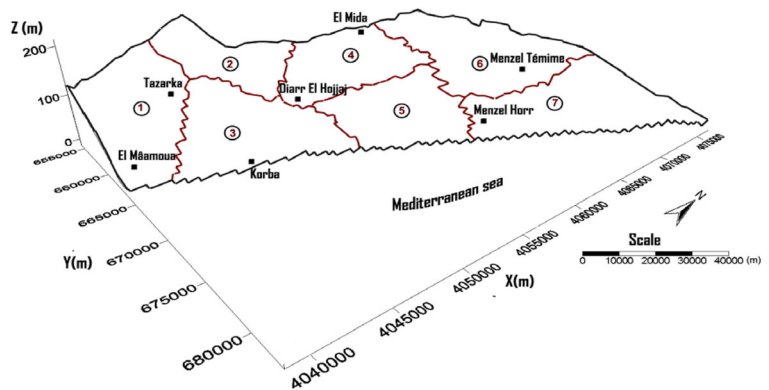
The discharge into the sea in the transit state in 2014 decreased to about 8.03 Mm^3/year (10.5% of the outflow), while seawater intrusion reached 26.68 Mm^3/year (35% of the inflow). Also, precipitation recharge contributed 43.5% of the inflow (33.10 Mm^3/year) which was enough to counteract the seawater intrusion. In addition, groundwater overexploitation caused an additional 5.15 Mm^3/year of seawater inflow into the groundwater as compared with the steady state water budget. It also caused a reduction of the submarine discharge of 9.74 Mm^3/year. Comparing 1965 and 2014 mass balances, there is clear evidence of unsustainable groundwater use. However, the total system storage does not appear to change significantly (Table 4). Overall, the calibrated/verified 3D model is able to simulate TDS and hydraulic head fluctuations at a level deemed sufficient to evaluate the impact of future management scenarios on the groundwater system.
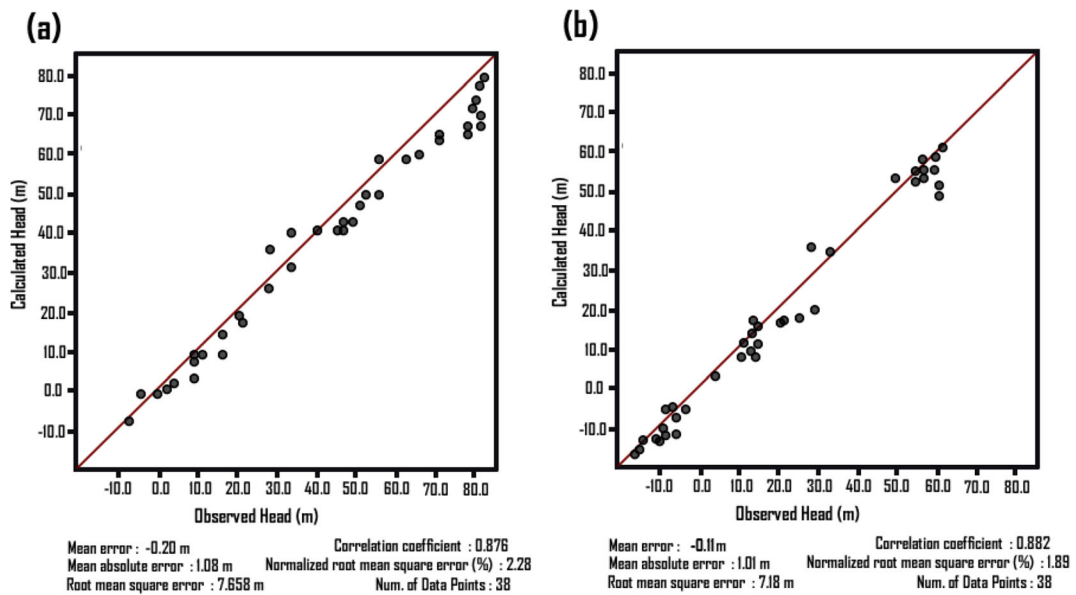
Simulation results

Effects on groundwater level

A quantitative understanding of the rate and extent of seawater intrusion into the Korba aquifer is an important prerequisite for characterizing the region's long-term vulnerability to groundwater quantity and quality concerns. Previous investigations using time-domain electromagnetic (TDEM) method, Vertical Electrical Sounding (VES), and Electrical Resistivity Tomography (ERT) have improved the estimation of Korba aquifer's freshwater-saltwater transition zone (Kouzana et al. 2010; Ziadi et al. 2017). These studies have illustrated surface water-groundwater connection at wadis, contributing to salinization due to infiltration of high-TDS water from the riverbed. Building on these investigations along with other previous efforts to model the Korba system (e.g., Paniconi et al. 2001; Kerrou et al. 2010), we projected the movement of the salt front under three groundwater management scenarios through a series of predictive pumping simulations.

Fig. 9 Derived seven distinct hydrogeological domains during modeling procedure

(a)

(b)

Mean error : −0.20 m   Correlation coefficient : 0.876
Mean absolute error : 1.08 m   Normalized root mean square error (%) : 2.28
Root mean square error : 7.658 m   Num. of Data Points : 38

Mean error : −0.11 m   Correlation coefficient : 0.882
Mean absolute error : 1.01 m   Normalized root mean square error (%) : 1.89
Root mean square error : 7.18 m   Num. of Data Points : 38

Fig. 10 Observed versus calculated heads: **a** steady sate 1965 and **b** transit state 2014

Scenario 1 illustrates the Korba aquifer system's vulnerability to the current unsustainable groundwater exploitation, which results in slow but extensive groundwater table decline. For this scenario (Fig. 14b), it was assumed that the 2014 groundwater extractions (68 Mm^3/year) will remain the same until 2050. The resulting drawdown contour map shows a cone of depression 15 m below sea level. Maximum drawdown occurs in the center and close to the shoreline where there are extensive agricultural activities with the largest

pumping rate. The projected groundwater level in 2050 is − 2.5 m lower than the 2014 level (Table 5), showing a slow decline rate (0.06 m/year). Subsequently, the Korba aquifer's negative water balance will be aggravated due to the continuous groundwater level decrease. This continuous water level decrease accelerates the seawater intrusion by reversing the hydraulic gradients (Zghibi et al. 2011; Siarkos and Latinopoulos 2016).

Given the historical trend of increasing groundwater extraction to support socio-economic growth, it is imperative to assess the regional groundwater drawdown problem under a growing water demand scenario. Thus, for scenario 2 (Fig. 14c), the abstractions were assumed to increase by 25% compared to the business-as-usual scenario (scenario 1) due to increased agricultural water demand. The greatest decline of groundwater level was observed in the center and near the eastern boundary. By 2050, the cone of depression, located approximately 5 km from the coast, drops to about 20 m below sea level showing a relatively fast decline rate of 0.50 m/year. Consequently, groundwater level was about 5.50 m below sea level for the whole simulation period (Table 5). Approximately 70% of the total groundwater withdrawal occurred in a small critical zone (21% of the total area) in the central part with several piezometric depression cones. Although scenario 2 is extreme, the critical zone is clearly vulnerable to changes in withdrawal, indicating that future groundwater allocations should be carefully regulated.

Table 3 Model performance evaluation

| Phase	Criterion	Steady state	Transit state		
			Mean	Min	Max
Calibration	ME (m)	− 0.20	0.43	0.10	0.81
	MAE(m)	1.08	1.09	0.88	1.11
	RMSE (m)	7.66	7.23	7.05	7.51
	NRMSE (%)	2.28	2.02	0.88	2.61
	γ	0.895	0.89	0.80	0.91
	R^2	0.88	0.81	0.87	0.89
Verification	ME (m)	− 0.11			
	MAE(m)	1.01			
	RMSE (m)	7.18			
	NRMSE (%)	1.89			
	γ	0.88			
	R^2	0.88			
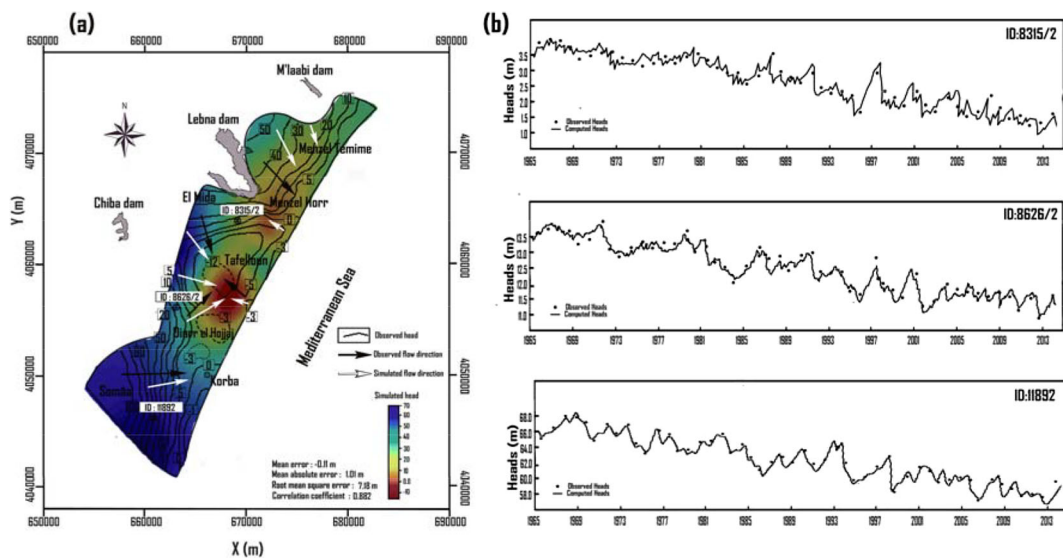
Fig. 11 **a** Simulated water level in the year 2014 and **b** Fitted observed and computed hydraulic heads time series at three monitoring wells (ID: 8315/2, 8626/2, and 11892) as result of model calibration

The third scenario (Fig. 14d) provides insights into curbing the groundwater table decline and seawater intrusion through remediation countermeasures that decrease groundwater extraction from the existing wells by 25%, which requires alternative water resources in the region. This groundwater conservation scenario reveals that groundwater extraction should be reduced by 17 Mm^3/year in order to mitigate the seawater intrusion. Simulation results under this scenario indicate that it will take at least 43 years to push back the saltwater front along the coastline by about 25%. Thus, the coastal aquifer remediation will be difficult but necessary for keeping the seawater/freshwater equilibrium closer to the sea. Efforts to mitigate further seawater contamination and remediate salty groundwater should focus on the northern and southern parts of the aquifer.

Effects on freshwater-saltwater transition zone

The TDS concentration increases under the first scenario (Fig. 15). The seawater front expands overtime (to year 2050) as indicated by the TDS isolines at 2.0 kg/m^3 increments, making groundwater quality unsuitable for agricultural and urban use. Evidently, the drawdown
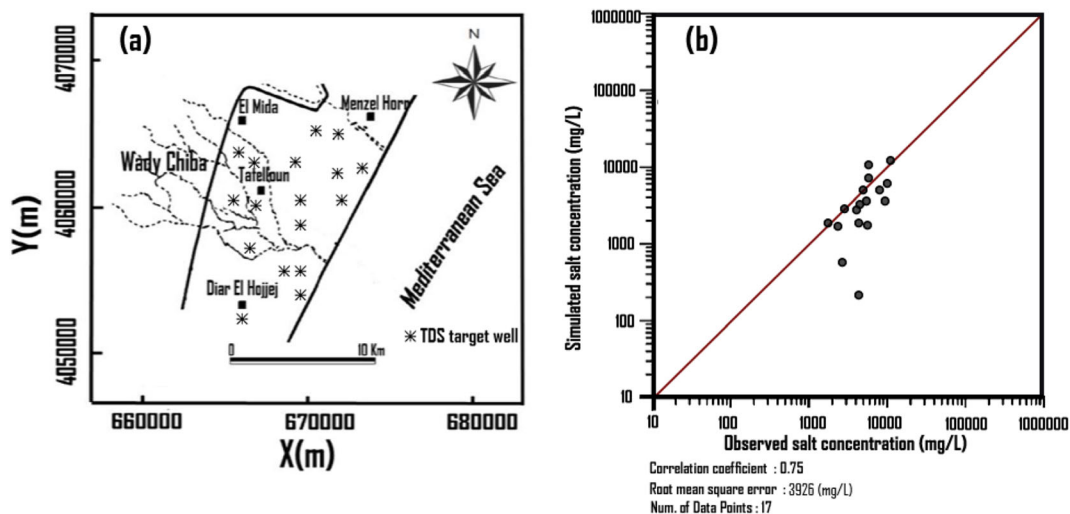
Fig. 12 **a** Locations of 17 monitoring wells used in transport modeling and **b** observed versus simulated TDS
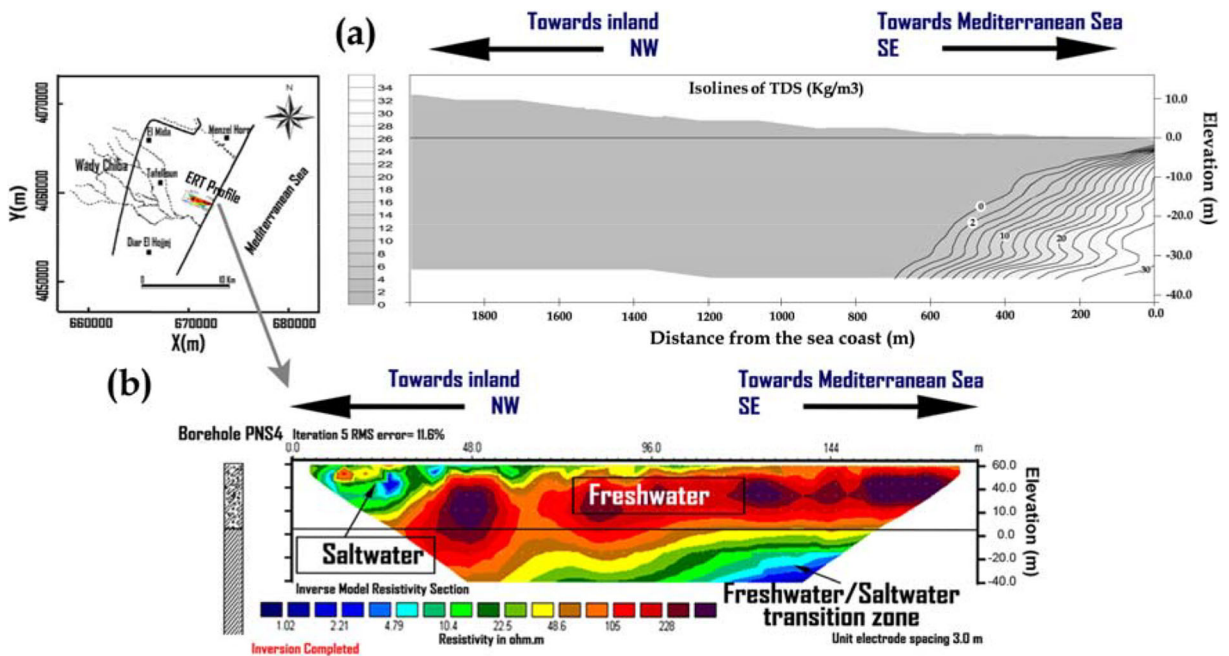
Fig. 13 **a** Isolines of calculated TDS concentration (kg/m³) by MT3DMS in year 2014 and **b** ERT profile along geoelectrical cross section and its location

of the water table below the sea level caused by increasing pumping stresses (Fig. 15a) led to further inland propagation of the saltwater wedge. The combination of the inland reversal of flow direction and saltwater upconing mechanism due to groundwater pumping causes seawater intrusion rates to be on the order of 100 m/year (Kerrou et al. 2010), which corresponds to about 7 Mm³/year of seawater flux entering the aquifer.

By comparing the projected landward movement of the seawater wedge in 2050 with the state of the aquifer in 2014 (Fig. 15b), the total seawater intrusion is expected to reach 1.8 km. This means that the saltwater front will migrate inland an additional distance of 1 km over a 43-year period as compared with 2014 when the seawater front is at a maximum

distance of 0.8 km from the shoreline. This is not surprising because of the magnitude of the inland inversion of the hydraulic gradient, which causes significant mixing of the TDS-rich Mediterranean Sea water in the aquifer system by the year 2050. In addition, the exchange with the sea will occur unidirectionally landward. Under scenario 1, the inflow from the sea increases slightly from about 26.68 Mm³/year in 2014 to 32.02 Mm³/year in 2050.

The increase in groundwater extraction by 25% under scenario 2 resulted in a decrease in the mean hydraulic head level by 0.5 m/year, creating the worst TDS condition. Consequently, the longitudinal extent of the 2.0 kg/m³ TDS isoline was around 3 km (Fig. 16a) and

Table 4 Groundwater mass balance of the transient flow model before exploitation (1965) and in 2014

| Year	In (Mm³/year)							Out (Mm³/year)			Storage change (ΔS)	
	Storage	Lateral recharge	Sea	Recharge from TWW since 2008	Rainfall recharge	Recharge from Lebna Dam since 1986	Total in	Storage	Wells	Sea	Total out	
1965	0.00	3.76	2.88	0.00	29.82	0.00	36.46	0.00	0.00	36.42	36.42	0.04
2014	7.13	3.76	26.68	1.7	33.10	3.73	76.1	0.00	68	8.03	76.03	0.07
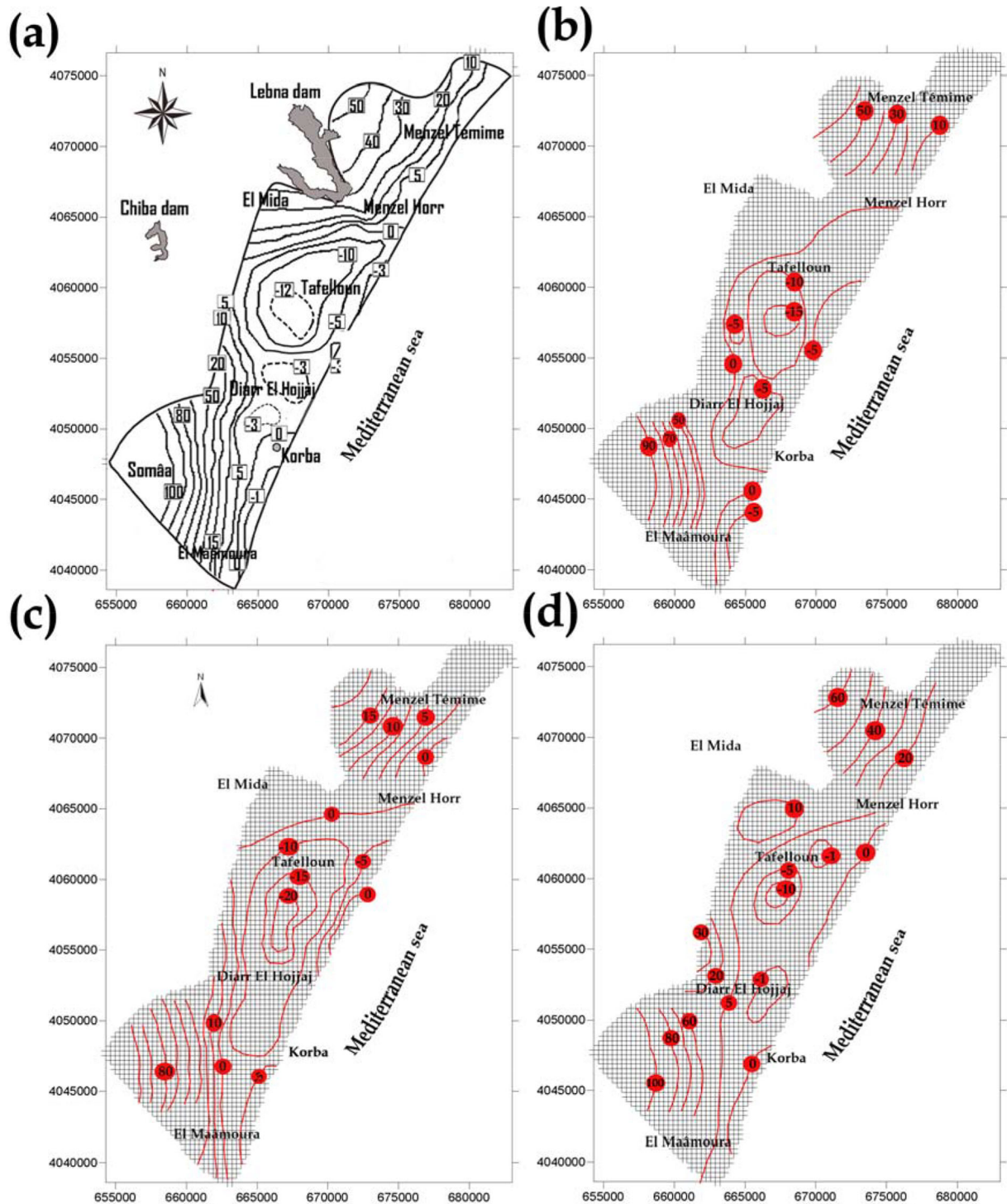
Fig. 14 Water table elevation for the years 2014 and 2050: **a** Potentiometric level at initial year 2014, **b** drawdown isopleths of scenario 1, **c** of scenario 2 and **d** of scenario 3

**Table 5** Groundwater management scenario results

Scenario	Description	Groundwater level change (m)			
		Mean	Max	Min	SD
1	Business as usual	− 2.5	− 4	− 0.2	5.2
2	25% increase in GW pumping	− 5.5	− 8.02	− 0.5	4.7
3	25% decrease in GW pumping	0.5	1.96	0.00	3.03

the inland seawater intrusion was approximately 2.5 km (Fig. 16b). Due to the abstraction effect, the inflow from the sea for the year 2050 will become very significant (i.e., more than 56.12 Mm^3/year). The relative salt concentration distribution shows that the maximum seawater intrusion is registered near Korba City and below the central part of the study area between Diarr El Hojjaj and Mida villages. This saline water plume extension
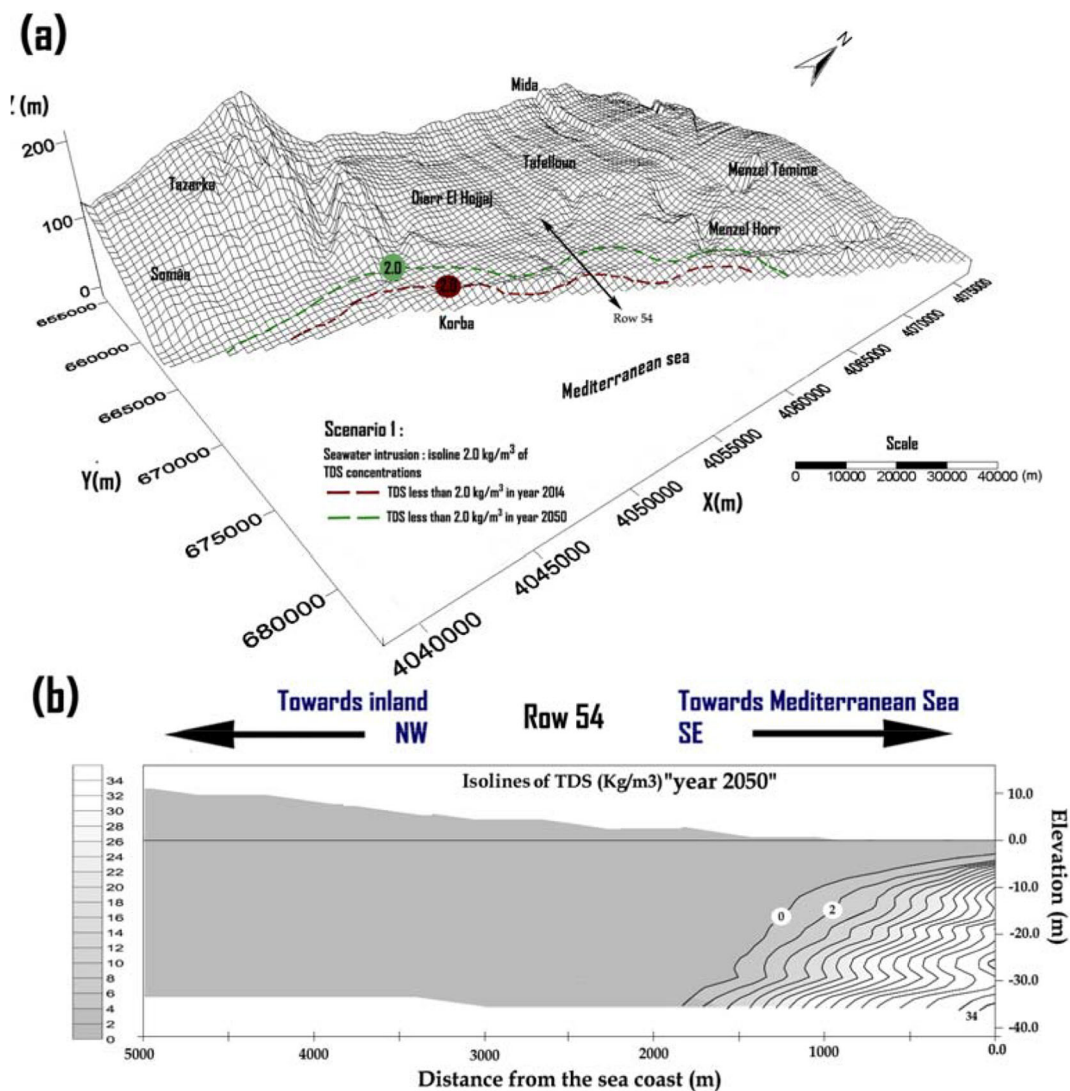
Fig. 15 Scenario 1: **a** Relative salt concentration distribution at the beginning (2014) and the end (2050) of the simulation period and **b** cross sections of year 2050
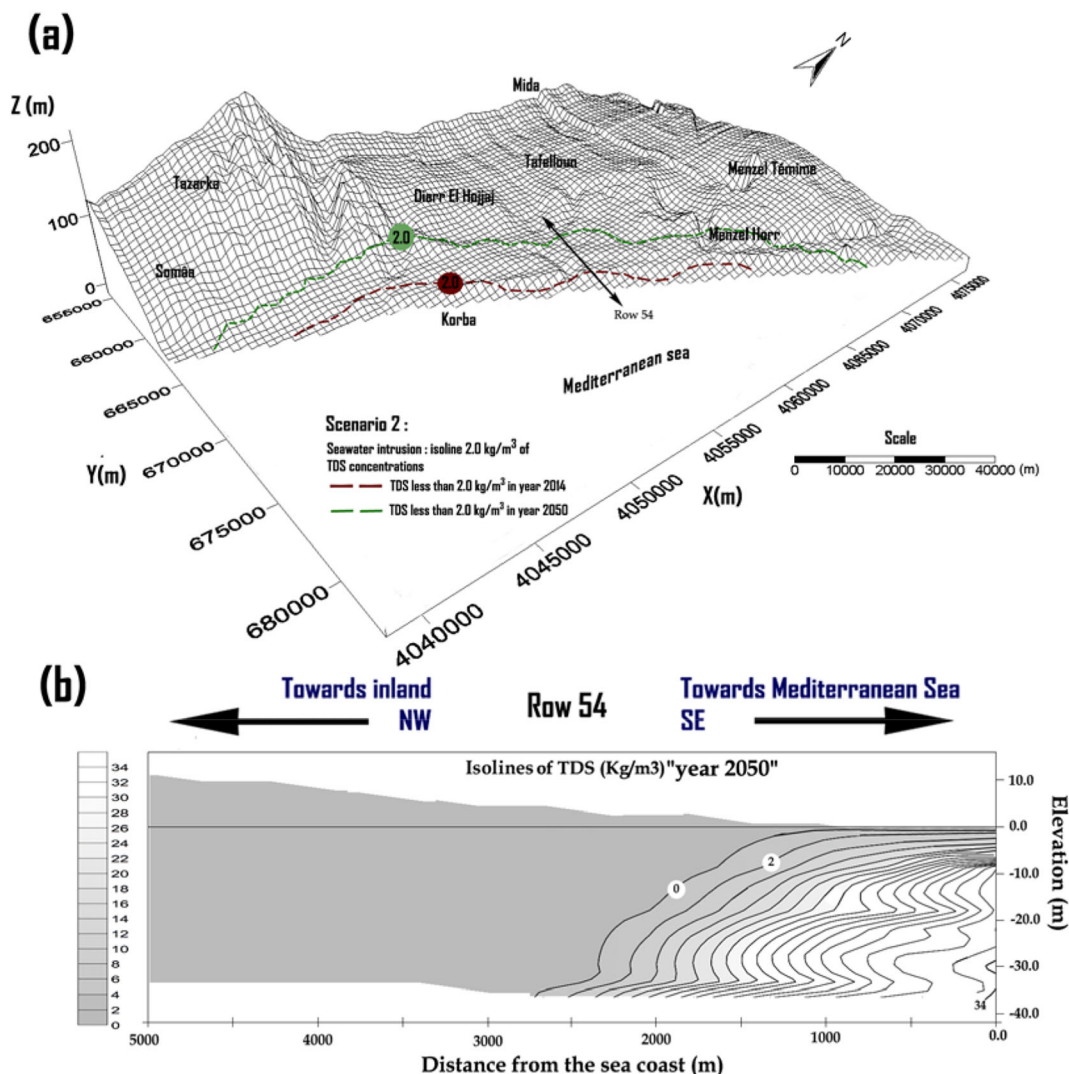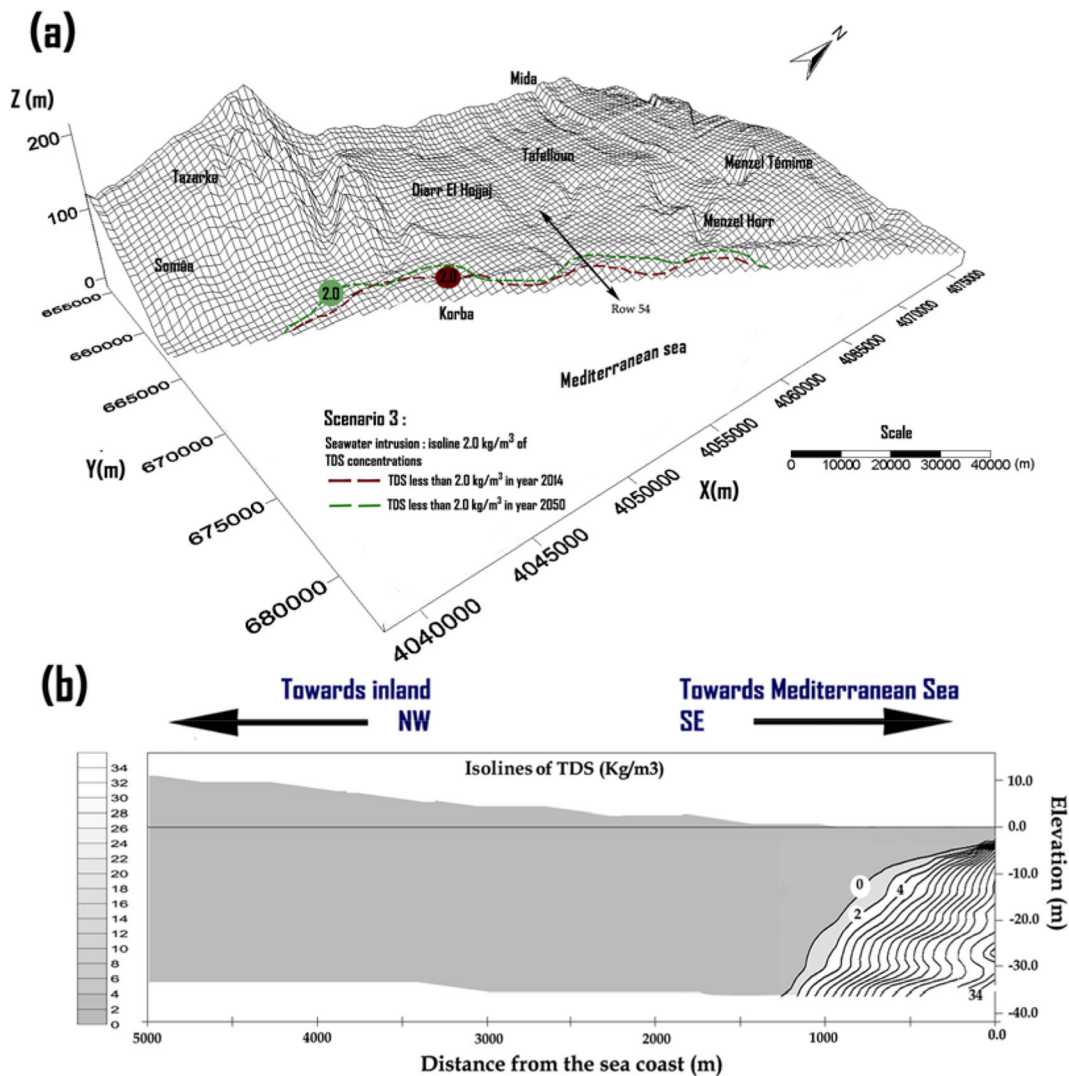
Fig. 16 Scenario 2: **a** Relative salt concentration distribution at the beginning (2014) and the end (2050) of the simulation period and **b** cross sections of year 2050

can be explained by high transmissivity of the lithology of the Pliocene formations with dominant yellow sand and sandstone intercalations and the sufficiently porous media constituting the river beds (Chekirbane et al. 2015).

Finally, scenario 3 showed the effect on the Korba groundwater due to the gradual reduction of the pumping rates over the aquifer by 25% until 2050. The 2.0 kg/m^3 TDS line advanced a few hundred meters inland as compared with scenario 1 (Fig. 17a), illustrating the effectiveness of mitigation measures to protect the coastal aquifer during a 43-year period, although this approach will not stop the saltwater intrusion altogether. The vertical

movement of the TDS plume (i.e., 2 g/L TDS lines) is relatively small in comparison with the movement in the transversal direction. Prohibiting pumping close to the seawater affected areas, optimizing pumping rates to increase water use efficiency, and installing more artificial recharge sites (e.g., using treated wastewater) will help mitigate the saltwater intrusion problem in the Korba region.

The presented groundwater modeling approach and scenario results inform sustainable groundwater management in the face of increasing salinity in the coastal aquifer. Quantification of groundwater recharge and pumping rates as well as a detailed hydrogeological mapping (Dinka et al. 2014) should

Fig. 17 Scenario 3: **a** Relative salt concentration distribution at the beginning (2014) and the end (2050) of the simulation period and **b** cross sections of year 2050

be prioritized to improve the evaluation of salt front movement in the Korba aquifer system and other costal aquifers in Tunisia. Future work can focus of representing land surface hydrology using distributed watershed simulation models (e.g., Soil and Water Assessment Tool (SWAT; Arnold et al. 1998)) coupled with the MODFLOW model of the aquifer to examine potential effects of climate change and urbanization (Akbarpour and Niksokhan 2018) on groundwater balance. The presented numerical modeling approach is transferrable to other coastal aquifers in Tunisia and around the world with similar groundwater management challenges as the Korba case.

Conclusions

Groundwater table decline and seawater intrusion pose a challenge to sustainable irrigated agriculture in Tunisia's coastal plains. This paper presented a coupled numerical groundwater modeling approach to simulate the rate and extent of seawater intrusion into Korba aquifer, an unconfined coastal aquifer in Tunisia's Cap-Bon Peninsula. We linked MODFLOW-2000 and MT3DMS models within the Groundwater Modeling System (GMS 6.5) to conduct a comprehensive groundwater balance analysis. The model illustrates groundwater table decline under steady and transient states across the aquifer,

including a concentric depression 12 m below sea level in the central part of the region approximately 3 km from the shoreline and along the Mediterranean coast where the hydraulic gradients were reversed. The precipitation recharge contributes 43.5% of the inflow to the aquifer system, which is enough to counteract the intrusion of about 26.68 Mm^3/year of seawater. However, groundwater overexploitation caused an additional 5.15 Mm^3/year of seawater inflow into the aquifer, necessitating the development and implementation of actions to minimize, if not prevent, the expansion of seawater intrusion and its possible threats to the region.

We projected the aquifer behavior up to 2050 under three groundwater management schemes through a series of predictive pumping simulations. Under projected business-as-usual groundwater management scenario, a significant volume of seawater will enter the aquifer, mainly in the central part due to extensive agricultural activities. By 2050, the saltwater wedge will likely move about 1.8 km inland compared to its location in 2014. A 25% increase in groundwater extraction (scenario 2) will intensify the groundwater drawdown (e.g., 0.50 m/year) forming a cone of depression 20 m below sea level. The saltwater front can migrate 2.5 km inland along a 3-km stretch of the coastline. By contrast, reducing groundwater extraction by 25% (scenario 3) can effectively curb the saltwater intrusion by establishing the saltwater-freshwater dynamic equilibrium closer to the sea. Under this scenario, it will take 43 years to push the salt front back by 25% compared to its location under scenario 1. The results and the presented saltwater intrusion assessment framework inform sustainable groundwater management in the Korba plain with important implications for other vulnerable agricultural costal aquifers in Tunisia and around the world.

References

Ahmad, Z., Kausar, R., & Ahmad, I. (2010). Implications of depletion of groundwater levels in three layered aquifers and its management to optimize the supply demand in the urban settlement near Kahota Industrial Triangle area, Islamabad, Pakistan. *Environmental Monitoring and Assessment, 166*, 41–55.

Akbarpour, S., & Niksokhan, M. H. (2018). Investigating effects of climate change, urbanization, and sea level changes on groundwater resources in a coastal aquifer: An integrated assessment. *Environmental Monitoring and Assessment, 190*, 579.

Anderson, E. R., Hill, M. C. (2000). MODFLOW 2000, the U.S. Geological Survey Modular Ground-Water Model – Documentation of the Hydrogeologic-Unit Flow (HUF) Package. *United States Geological Survey Open-File Report* 00-342. United States Geological Survey, Reston, VA.

Anderson, M. P., & Woessner, W. M. (1992). Applied groundwater modeling: Simulation of flow and advective transport. *Academic., 4*, 381p.

AQUAVEO. (2018). GMS - groundwater modeling system– create 3D models with speed & simplicity using GMS - the most intuitive & capable platform for groundwater & subsurface simulations. https://www.aquaveo.com/software/gms-groundwater-modeling-system-introduction.

Arnold, J. G., Srinivasan, R., Muttiah, R. S., & Williams, J. R. (1998). Large area hydrologic modeling and assessment part I: Model development. *Journal of the American Water Resources Association, 34*(1), 73–89.

Barth, C., Krause, P., Boyle, D.P., Markstrom, S. L. (2007). Hydrological modeling of a groundwater dominated watershed using a loosely coupled modeling approach. International Congress on Modeling and Simulation, *Modeling and Simulation Society of Australia and New Zealand Inc.*, 601–607.

Bear, J., & Cheng, A. (2010). *Modeling groundwater flow and contaminant transport*. Heidelberg: Springer.

Bear, J., Cheng, A. H. D., Sorek, S., Ouazar, D., & Herrera, I. (1999). *Seawater intrusion in coastal aquifers-concepts, methods and practices*. Dordrecht: Kluwer.

CCI Cap-Bon. (2018). Chambre de Commerce et d'Industrie du Cap-Bon, Tunisia [online]. Available from: http://www.ccicapbon.org.tn.

Chandio, A. S., & Lee, T. S. (2012). Managing saline water intrusion in the lower Indus Basin aquifer. *Water Resources Management, 26*, 1555–1576.

Chekirbane, A., Tsujimura, M., Kawachi, A., Isoda, H., Tarhouni, J., & Benalaya, A. (2015). 3D simulation of a multi-stressed coastal aquifer, northeast of Tunisia: Salt transport processes and remediation scenarios. *Environmental Earth Sciences, 73*, 1427–1442.

Chekirbane, A., Tsujimura, M., Lachaal, F., Khadhar, S., Mlayah, A., Kawachi, A., Isoda, H., Tarhouni, J., & Benalaya, A. (2016). Quantification of groundwater - saline surface water interaction in a small coastal plain in North-East Tunisia using multivariate statistical analysis and geophysical method. *Water Environment Research, 12*, 2292–2308.

Chen, Z., Hartmann, A., & Goldscheider, N. (2017). A new approach to evaluate spatiotemporal dynamics of controlling parameters in distributed environmental models. *Environmental Modeling and Software, 87*, 1–16.

Cobaner, M., Yurtal, R., Dogan, A., & Motz, L. H. (2012). Three dimensional simulation of seawater intrusion in coastal aquifers: a case study in the Goksu Deltaic Plain. *Journal of Hydrology, 465*, 262–280.

Coro, G., Vilas, L. G., Magliozzi, C., Ellenbroek, A., Scarponi, P., & Pagano, P. (2018). Forecasting the ongoing invasion of Lagocephalus sceleratus in the Mediterranean Sea. *Ecological Modeling, 371*, 37–49.

Diersch, H. G. (1996). *Interactive, graphics-based finite element simulation system FEFLOW for modeling groundwater flow, contaminant mass and heat transport.* Berlin: WASY Institute for Water Resource Planning and System Research Ltd.

Dinka, M. O., Loiskandl, W., & Ndambuki, J. M. (2014). Hydrologic modelling for Lake Basaka: development and application of a conceptual water budget model. *Environmental Monitoring and Assessment, 186*, 5363–5379.

Doherty, J. L. (2000). *PEST: Model independent parameter estimation. User Manual* (4th ed.). Watermark Numerical Computing: Brisbane.

Don, N. C., Hang, N. T. M., Araki, H., Yamanishi, H., & Koga, K. (2006). Groundwater resources and management for paddy field irrigation and associated environmental problems in an alluvial coastal lowland plain. *Agricultural Water Management, 84*, 295–304.

Doulgeris, C., & Zissis, T. (2014). 3D variable density flow simulation to evaluate pumping schemes in coastal aquifers. *Water Resources Management., 28*, 4943–4956.

Droogers, P., Immerzeel, W. W., Terink, W., Hoogeveen, J., Bierkens, M. F. P., Van Beek, L. P. H., & Debele, B. (2012). Water resources trends in Middle East and North Africa towards 2050. *Hydrology and Earth System Sciences, 16*, 1–18.

El Ayni, F., Manoli, E., Cherif, S., & Jrad, A. (2013). Deterioration of a Tunisian coastal aquifer due to agricultural activities and possible approaches for better water management. *Water and Environment Journal, 27*, 348–361.

Ennabli, M. (1980). Etude hydrogélogique des aquifères du Nord-Est de la Tunisie pour une gestion intégrée des ressources en eau. Thesis (PhD), Nice University, France.

Giambastiani, B. M. S., Antonellini, M., Oude Essink, G. H. P., & Stuurman, R. J. (2007). Saltwater intrusion in the unconfined coastal aquifer of Ravenna (Italy): a numerical model. *Journal of Hydrology, 340*, 91–104.

Harbaugh, A. W., Banta, E. R., Hill, M. C., McDonald, M. G. (2000). The U.S. Geological Survey's Modular Ground Water Flow Model e User Guide to Modularization Concepts and the Ground Water Flow Process. U.S. Geological Survey. Open-File Report 00-92.

Hill, M. C., & Tiedeman, C. R. (2006). *Effective groundwater model calibration: With analysis of data, sensitivities, predictions, and uncertainty.* Hoboken: John Wiley & Sons.

Kajenthira, A., Siddiqi, A., & Anadon, L. D. (2012). A new case for promoting wastewater reuse in Saudi Arabia: Bringing energy into the water equation. *Journal of Environmental Management, 102*, 184–192.

Kamali, A., & Niksokhan, M. H. (2017). Multi-objective optimization for sustainable groundwater management by developing of coupled quantity-quality simulation-optimization model. *Journal of Hydroinformatics, 19*, 973–992.

Kerrou, J., Renard, P., & Tarhouni, J. (2010). Status of the Korba groundwater resources (Tunisia): Observations and three-dimensional modeling of seawater intrusion. *Hydrogeology Journal, 18*, 1173–1190.

Kotnik, J., Horvat, M., Begu, E., Shlyapnikov, Y., Sprovieri, F., & Pirrone, N. (2017). Dissolved gaseous mercury (DGM) in the Mediterranean Sea: Spatial and temporal trends. *Marine Chemistry, 193*, 8–19.

Kouzana, L., Benassi, R., Ben Mammou, A., & Sfar felfoul, M. (2010). Geophysical and geochemical study of the seawater intrusion in Mediterranean semi arid zones. Case of the Korba coastal aquifer (Cap-Bon, Tunisia). *Journal of African Earth Sciences, 58*, 242–254.

Lachaal, F., Chekirbane, A., Chargui, S., Sellami, H., Tsujimura, M., Hezzi, H., Jelassi, F., & Mlayah, A. (2016). Water resources management strategies and its implications on hydrodynamic and hydrochemical changes of coastal groundwater: Case of Grombalia shallow aquifer, NE Tunisia. *Journal of African Earth Sciences, 124*, 171–188.

Langevin, C. D., & Guo, W. (2006). MODFLOW/MT3DMS–based simulation of variable-density ground water flow and transport. *GroundWater, 44*, 339–351.

Liang, H., Qin, W., Hu, K., Tao, H., & Li, B. (2019). Modeling groundwater level dynamics under different cropping systems and developing groundwater neutral systems in the North China Plain. *Agricultural Water Management, 213*, 732–741.

Mao, X., Prommer, H., Barry, D. A., Langevin, C. D., Panteleit, B., & Li, L. (2006). Three-dimensional model for multi-component reactive transport with variable density groundwater flow. *Environmental Modeling & Software, 21*, 615–628.

McDonald, M. G., & Harbaugh, A. W. (1988). *A modular three-dimensional finite difference ground-water flow model. Techniques of Water Resources Investigations, Book 6.* USGS: Reston, VA 586 pp.

Neitsch, S. L., Arnold, J. G., Kiniry, J. R., Williams, J. R. (2011). *Soil and water assessment tool theoretical documentation version 2009.* Texas Water Resources Institute.

Nettasana, T., Craig, J., & Tolson, B. (2012). Conceptual and numerical models for sustainable groundwater management in the Thaphra area, Chi River Basin, Thailand. *Hydrogeology Journal, 20*, 1355–1374.

Paniconi, C., Khlaifi, I., Lecca, G., Giacomelli, A., & Tarhouni, J. (2001). A modeling study of sea water intrusion in the Korba coastal plain, Tunisia. *Physics and Chemistry of the Earth (B), 26*, 345–351.

Pham, H. V., & Lee, S. I. (2015). Assessment of seawater intrusion potential from sealevel rise and groundwater extraction in a coastal aquifer. *Desalination and Water Treatment, 53*, 2324–2338.

Post, V. E. A. (2005). Fresh and saline groundwater interaction in coastal aquifers: is our technology ready for the problems ahead? *Hydrogeology Journal, 13*, 120–123.

Qahman, K., & Larabi, A. (2006). Evaluation and numerical modeling of seawater intrusion in the Gaza aquifer (Palestine*). Hydrogeology Journal, 14*, 713–728.

Rahman, M. A., Rusteberg, R., Salah Uddin, M., Lutz, A., Abu Saada, M., & Sauter, M. (2013). An integrated study of spatial multicriteria analysis and mathematical modeling for managed aquifer recharge site suitability mapping and site ranking at Northern Gaza coastal aquifer. *Journal of Environmental Management, 124*, 25–39.

Salcedo-Sànchez, E. R., Vicenta-Esteller, M., Garrido-Hoyos, S. E., & Martinez-Morales, M. (2013). Groundwater optimization model for sustainable management of the Valley of Puebla aquifer, Mexico. *Environmental Earth Sciences, 70*, 337–351.

Siarkos, L., & Latinopoulos, P. (2016). Modeling seawater intrusion in overexploited aquifers in the absence of sufficient data: Application to the aquifer of Nea Moudania, northern Greece. *Hydrogeology Journal, 24*, 2123–2141.

Slama, F., & Bouhlila, R. (2016). Multivariate statistical analysis and hydrogeochemical modeling of seawater-freshwater mixing along selected flow paths: Case of Korba coastal aquifer Tunisia. *Estuarine, Coastal and Shelf Science, 198*, 636–647.

Tsujimura, M., Chekirbane, A., Tarhouni, J. (2014). Water Resources in Tunisia. Chapter 11 in Sustainable North African Society: Exploring the Seeds and Resources for Innovation. *NOVA Sci. Publ.*. ISBN: 978-1-63463-220-1. 275p.

UN-Water: World Water Development Report. (2014). *Water Energy*. Paris: UNESCO.

Verdier, F. (2011). MENA Regional Water Outlook Part II: Desalination using renewable energy, http://www.dlr.de/tt/Portaldata/41/Resources/dokumente/institut/system/projects/MENA_REGIONAL_WATER_OUTLOOK.pdf.

Voss, C. I., & Souza, W. R. (1987). Variable density flow and solute transport simulation of regional aquifers containing a narrow freshwater-saltwater transition zone. *Water Resources Research, 23*, 1851–1866.

Werner, A. D., & Gallagher, M. R. (2006). Characterisation of seawater intrusion in the Pioneer Valley, Australia using hydrochemistry and three dimensional numerical modeling. *Hydrogeology Journal, 14*, 1452–1469.

Werner, A. D., Bakker, M., Post, V. E. A., Vandenbohede, A., Lu, C., Ataie-Ashtiani, B., Simmons, C. T., & Barry, D. A. (2013). Seawater intrusion processes, investigation and management: Recent advances and future challenges. *Advances in Water Resources, 51*, 3–26.

Xiaobin, Z. (2003). Groundwater modeling system (GMS) software. *Hydrogeology and Engineering Geology, 5*, 53–55.

Xu, Z., Hu, B. X., Davis, H., & Kish, S. (2015). Numerical study of groundwater flow cycling controlled by seawater/freshwater interaction in a coastal karst aquifer through conduit network using CFPv2. *Journal of Contaminant Hydrology, 182*, 131–145.

Xu, Z., Hu, B. X., & Ye, M. (2018). Numerical modeling and sensitivity analysis of seawater intrusion in a dual-permeability coastal karst aquifer with conduit networks. *Hydrology and Earth System Sciences, 22*, 221–239.

Yazdanpanah, M., Hayati, D., Hochrainer-Stigler, S., & Zamani, H. G. (2014). Understanding farmers' intention and behavior regarding water conservation in the Middle-East and North Africa: A case study in Iran. *Journal of Environmental Management, 135*, 63–72.

Zghibi, A., Zouhri, L., & Tarhouni, J. (2011). Groundwater modeling and marine intrusion in the semi-arid systems (Cap-Bon, Tunisia). *Hydrological Processes, 25*, 1822–1836.

Zghibi, A., Merzougui, A., Zouhri, L., & Tarhouni, J. (2014a). Understanding groundwater chemistry using multivariate statistics techniques to the study of contamination in the Korba unconfined aquifer system of Cap-Bon (North-east of Tunisia). *Journal of African Earth Sciences, 89*, 1–15.

Zghibi, A., Merzougui, A., Zouhri, L., & Tarhouni, J. (2014b). Interaction between groundwater and seawater in the coastal aquifer of Cap-Bon in the semi-arid systems (north-east of Tunisia). *Carbonates and Evaporites, 29*, 309–326.

Zghibi, A., Merzougui, A., Chenini, I., Ergaieg, K., Zouhri, L., & Tarhouni, J. (2016). Groundwater vulnerability analysis of Tunisian coastal aquifer: an application of DRASTIC Index Method in GIS environment. *Groundwater for Sustainable Development, 2*, 169–181.

Ziadi, A., Tlatli-Hariga, N., & Tarhouni, J. (2017). Use of time-domain electromagnetic (TDEM) method to investigate seawater intrusion in the Lebna coastal aquifer of eastern Cap Bon, Tunisia. *Arabian Journal of Geosciences, 10*, 492.